

β^2 corrections to spherical EDF calculations for root-mean-square charge radii

B. Alex Brown and Kei Minamisono¹

¹*Department of Physics and Astronomy, FRIB Laboratory,
Michigan State University, East Lansing, MI 4284-1321, USA*

(Dated: April 15, 2022)

Root-mean-square charge radii are discussed in terms of spherical Energy Density Functional (EDF) models corrected for quadrupole deformations. Comparisons between experiment and theory are made for the absolute radii of all even-even nuclei, for the isotonic shift between cadmium and tin isotopes, the isotopic shifts of the calcium isotopes and the isotonic shift for nuclei with $N = 28$. We conclude that the data are well described in this approach, except for the sharp rise just after the neutron magic numbers.

INTRODUCTION

Root-mean-square (rms) charge radii of nuclei provide one of the most precise insights into nuclear structure. New experiments are being carried out on long chains of isotopes, and theoretical models are being improved, see [1], [2], [3] and references therein. Fig. (1) shows the measured rms charge radii for even-even nuclei from calcium to tellurium. One observes kinks in the isotopic trends at neutron numbers $N = 28$ and $N = 50$, as well as kinks in the isotonic trends at the proton numbers $Z = 28$ and $Z = 50$. In particular, the isotonic kink at $Z = 50$ results in a close spacing between the rms charge radii of cadmium and tin isotopes which is one of the topics of this paper.

We start with a comparison of the data to spherical energy-density functional (EDF) calculations using the 12 Skyrme functionals from Table I of [4]. As shown in Fig. 4 of [5], the main difference in the results for the rms charge radii for these 12 functionals is correlated with the effective mass. One group has $m^*/m \approx 1.0$. The results for $s8$ parameter set which is representative of this group are shown in Fig. (2). The other group has $m^*/m \approx 0.7 - 0.8$. The results for $s17$ parameter set which is representative of this group are shown in Fig. (3). These are carried out in a spherical basis with proton and neutron occupation numbers obtained from a self-consistent exact-pairing calculation [6] based on the $(J, T) = (0, 1)$ two-body matrix elements from configuration-interaction Hamiltonians used for the various mass regions. The calculations include the proton and neutron finite sizes and the relativistic spin-orbit corrections as described in [7].

The difference between experiment and the spherical calculations shows the well-known effect of nuclear deformation in between the magic numbers of 28, 50, 82 and 126. To account for deformation one can carry out deformed EDF calculations. Many such calculations give results at the energy minimum for a given β deformation. More advanced calculations include fluctuations around the minimum [8].

A different approach is to use the information con-

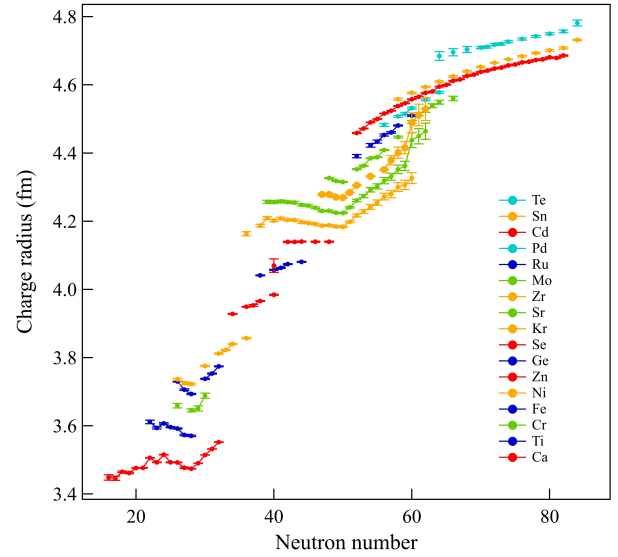


FIG. 1. Measured rms charge radii for even-even nuclei from $Z = 20$ (calcium) to $Z = 52$ (tellurium). The data are taken from compilations [9] and [10] with updated results for Ca [11], Fe [12], Ni [13], Cd [14], and Sn [15].

tained in the reduced transition probability $B(E\lambda)$ for the excitation of low-lying states to deduce an effective deformation parameter β (this includes the fluctuations) and then use the Bohr collective model to evaluate the change in the rms radius taking into account volume conservation as a function of deformation [16]. To order β^2 the mean-square radius is

$$\langle r^2 \rangle = \langle r^2 \rangle_0 \left[1 + \frac{5\beta^2}{4\pi} \right], \quad (1)$$

where

$$\langle r^2 \rangle_0 = \frac{3R_0^2}{5} \quad (2)$$

is the mean-square radius with no deformation, and

$$\beta^2 = \sum_{\lambda \geq 2} \beta_\lambda^2. \quad (3)$$

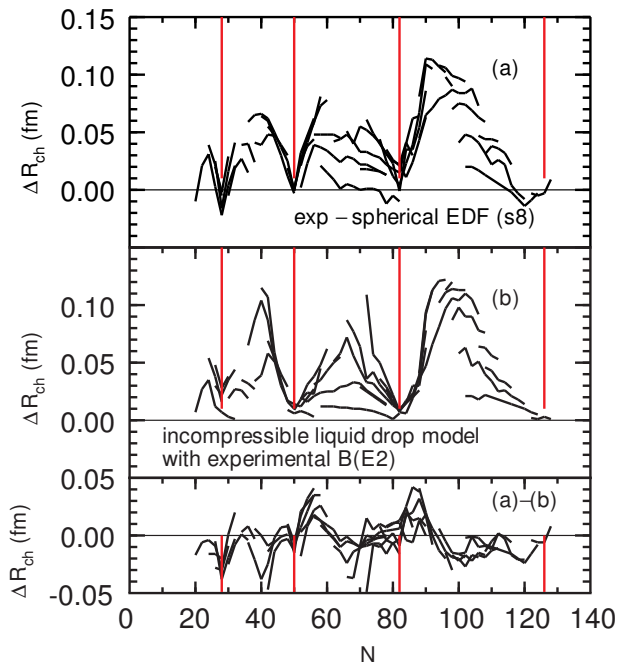


FIG. 2. (a) Difference between the experimental rms charge radii and those obtained in a spherical EDF calculation with the *S8* Skyrme functional. (b) The increase in the rms charge radii calculated with Eq. (1) using experimental $B(E2)$ values. (c) The difference between (a) and (b).

The proton β^2 is related to the $B(E\lambda, \uparrow)$ for 0^+ to λ^+ transitions (in units of e^2) by

$$\beta_\lambda^2 = \frac{B(E\lambda, \uparrow)}{\left[\frac{3}{4\pi} Z R_0^\lambda\right]^2}. \quad (4)$$

The operator for $E2$ is

$$\sum_i r_i^2 Y^{(2)}(\hat{r}_i) e_{iq} e \quad (5)$$

where e_q is the effective charge for protons ($q = p$) or neutrons ($q = n$). Fluctuations of the nuclear surface give corrections to the rms charge radii that have the same form as those of the Bohr deformed model [17].

We will assume equal (isoscalar) proton and neutron deformations. A more general expression for Eq. (1) with unequal proton and neutron deformations is given in [18]. Results for higher-order terms in Eq. (1) are given [19], [20], [21]. For $\lambda=2$, the next most important term is proportional to β_2^3 . For $|\beta| = 0.6$ this term gives about a 10% change to Eq. (1). This term depends on the sign of β which is often not measured, and it will not be included here.

The strength functions for $B(E2, \uparrow)$ are dominated by the low-lying excited 2^+ state and the high-lying giant quadrupole state. Low-lying excited states fall into three

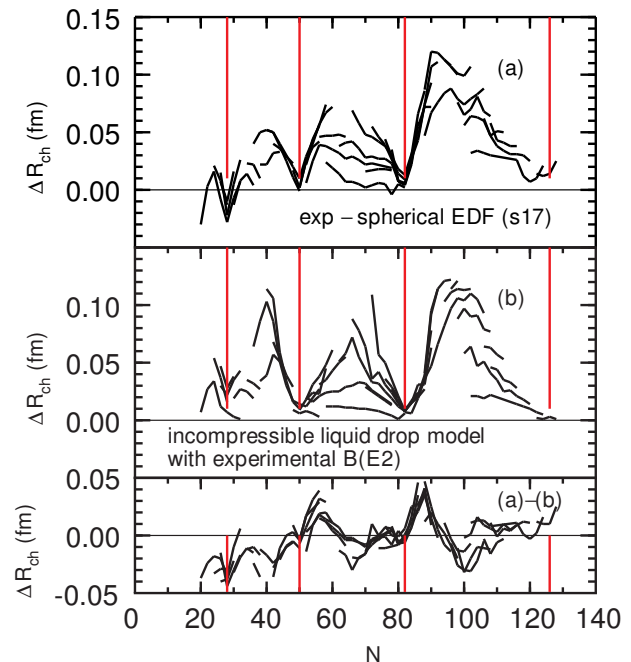


FIG. 3. (a) Difference between the experimental rms charge radii and those obtained in a spherical EDF calculation with the *s17* Skyrme functional. (b) The increase in the rms charge radii calculated with Eq. (1) using experimental $B(E2)$ values. (c) The difference between (a) and (b).

groups, (a) states in well deformed nuclei, (b) states in semi-magic nuclei formed from valence configurations below 2-3 MeV, and (c) states in doubly-magic nuclei formed by particle-hole excitations.

In this paper we compare experimental rms charge radii for nuclei on or near the semi-magic numbers with the results from three types of EDF calculations. The first is for the spherical EDF with parameters determined from bulk properties of doubly-magic nuclei [22], [23], [4], or from a large sample of nuclear bulk properties together with other observables resulting in the Sv-min set of EDF parameters [24]. The second is the same spherical calculations but supplemented with β_2^2 determined from experimental and/or calculated $B(E2)$ values of type (a) and (b) above. The third is the Fayans-type EDF [25], [26] with pairing terms added to provide an improved description of rms charge radii resulting in the Fy(Δr) set of parameters [3].

In the following we first consider the global comparison for even-even nuclei using experimental data for the $B(E2)$ values. We will call this the β_2^2 correction. We also look at the relative size of contributions to the rms radii coming from $\lambda=2, 3$ and 4. Next we look at the specific application to the isotonic shift between cadmium and tin to compare various approaches. Then we consider the isotopic shifts for $Z = 20$ (calcium) and the isotonic

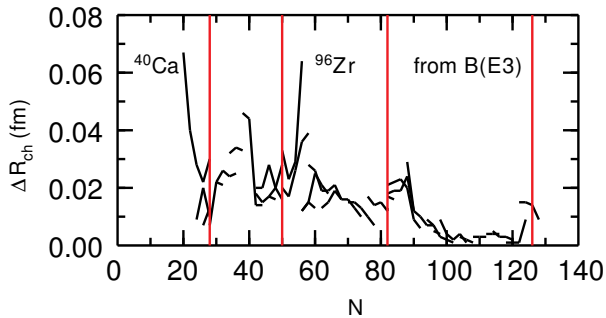


FIG. 4. Increase in the rms charge radii calculated with Eq. (1) using experimental $B(E3)$ [29].

shifts for $N = 28$ using experimental $B(E2)$ values. We also use configuration-mixing calculations for $Z = 20$ and $N = 28$ to calculate $\langle Q \cdot Q \rangle$ for both even-even and odd-even isotopes in order to explore the odd-even oscillations in the rms charge radii. At the end we discuss the problem for the increase in charge radii after the magic numbers and suggest possible solutions.

GLOBAL COMPARISONS

Using the compiled experimental $B(E2, 0^+ \rightarrow 2_1^+)$ values [27] the correction to the rms radii implied by Eq. (1) are shown in Figs. (2) and (3). The bottom panel of these figures show difference $R_{ch}(\text{experiment}) - R_{ch}(\text{theory}) - \Delta R_{ch}(\beta_2)$. $\Delta R_{ch}(\beta_2)$ is the calculated correction based on β_2^2 . The increase away from the magic numbers accounts for part of the kinks in the experimental radii at the magic numbers. There are some remaining deviations just after the magic numbers. For the region of the mass number $A = 100$, the $B(E2)$ for higher 2^+ states are typically less than about 5% of those for the first 2^+ state, see for example [28]. The contribution for the higher 2^+ states for the calcium isotopes and the $Z = 28$ isotones will be discussed below.

The next most important multiple is $\lambda=3$. The increase in the rms charge radii obtained from the experimental $B(E3, 0^+ \rightarrow 3_1^-)$ values [29] are shown in Fig. (4). In contrast to the dramatic shell effects observed for the $B(E2)$ in Figs. (2) and (3), the radius increase from the $B(E3)$ are rather flat. For the doubly-magic nuclei the $B(E3)$ are particle-hole excitation of the type (c) above. To the extent that the EDF parameters are determined to reproduce the rms radii of these doubly-magic nuclei, the effects of the $B(E3)$ contributions are contained in the EDF calculations. For nuclei in between the magic numbers, the $B(E3)$ is typically split over many low-lying states and their total contribution to the rms radii may be larger than that shown in Fig. (4). The largest ΔR_{ch} are observed for ^{40}Ca and ^{96}Zr . The implications of the

increase in $\Delta R_{ch}(E3)$ for ^{96}Zr and nuclei just after the magic numbers will be discussed at the end.

Results for the radii using the β_2 and β_4 obtained from the BSk27 EDF calculations [30] are shown in Fig. (5). β_4 accounts for about a third of the difference just after $N = 82$ shown in the bottom panels of Fig. (2) and (3).

ISOTONIC SHIFTS FOR THE CADMIUM AND TIN ISOTOPES

Modifications have been made to the Skyrme functionals to account for odd-even oscillators in the rms charge radii and the increase in radii after the magic numbers. The Fayans functionals add a pairing-type term to spherical EDF [25], [26]. The M3Y-P6a functional adds density-dependent spin-orbit and pairing terms to the M3Y-type functional [31].

As an example for isotonic shift in the rms charge radii, we consider the results for the cadmium and tin isotopes. These are shown in Fig. (6) using the experimental data and calculations given in [14] for cadmium and [15] for tin. The experimental data are compared to the spherical calculations with the Sv-min [24] EDF calculations given in the experimental papers [14], [15]. All 12 Skyrme functionals given in [4] give isotonic shifts similar to those shown for Sv-min. The experimental isotonic shift is closer to zero than to the standard Skyrme results.

In Fig. (6) The isotonic shifts are also compared to the results from the Fy($\Delta r, \text{HFB}$) functional given in [14], [15], and to the results obtained by adding the β_2^2 corrections using the experimental $B(E2)$ values from [32] to the Sv-min values. The error bars shown in Fig. (6) are from those given in [32] for the $B(E2)$ and from those given in [14] and [15] for the rms radii. The Sv-min plus β_2^2 corrections provide a reasonably good description of the data. The remaining differences between theory and experiment may be due to: (a) systematic uncertainties in the charge radii, (b) systematic uncertainties in the $B(E2)$ extracted from Coulex and/or lifetime measurements, (c) deficiencies in the Sv-min EDF, or (d) β_4^2 corrections.

ISOTOPIC SHIFTS FOR THE CALCIUM ISOTOPES

One of the most famous and challenging data for rms charge radii is that for the calcium isotopes where there is a strong odd-even oscillation in the rms charge radii with $^{42,44,46}\text{Ca}$ being relatively large compared to those for the "closed-shell" nuclei ^{40}Ca and ^{48}Ca . It is notable that the experimental rms charge radii of ^{40}Ca and ^{48}Ca are nearly the same [11]. This data has led to many theoretical ideas [33], [34], [35], [36], [37], [38], [39], [25],

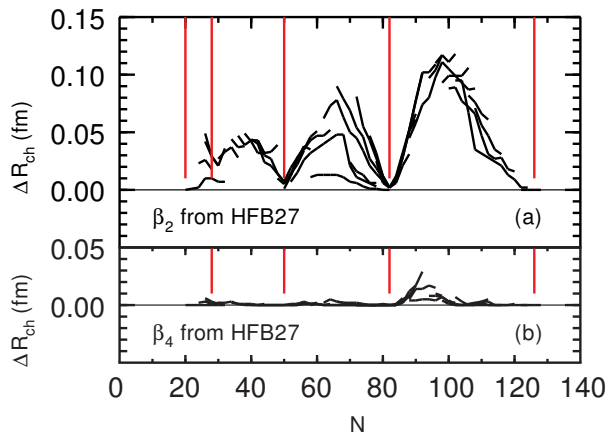


FIG. 5. (a) Increase in the rms charge radii calculated with Eq. (1) using the β_2 values obtained in a deformed EDF calculation with the HFB27 Skyrme functional. (b) Increase in the rms charge radii calculated with Eq. (1) using the β_4 values obtained in a deformed EDF calculations with the HFB27 Skyrme functional.

[26]. It was noted by Talmi [33] that a two-body effective operator for a correction to rms radii contains odd-even oscillations. The increase in the rms charge radii is correlated with an increase in the matter rms radii [40]. The increase in the rms radii for $^{42,44,46}\text{Ca}$ relative to ^{40}Ca and ^{48}Ca are in relatively good agreement with β_2^2 corrections obtained from the experimental $B(E2)$ values as shown in panels (a) and (b) of Fig. (7). The data are for ^{42}Ca [41], ^{44}Ca [42], ^{46}Ca and ^{50}Ca [43]. For ^{42}Ca we include the the $B(E2)$ for to the 2_2^+ state for which $B(E2, 0_1^+ \rightarrow 2_2^+)/B(E2, 0_1^+ \rightarrow 2_1^+) \approx 0.1$ [41]. The theoretical results from the $\text{Fy}(\Delta r, \text{HFB})$ calculations given in [44] are shown in panel (c) of Fig. (7).

These large $B(E2)$ cannot be described by calculations in the fp model space [45]. They are a result of admixtures from configurations with proton excitations from the sd shell to the pf shell. The configuration interaction (CI) calculations that include these cross shell excitation are challenging. In [37] the ZBM2 Hamiltonian for the $(1s_{1/2}, 0d_{3/2}, 0f_{7/2}, 1p_{3/2})$ model space was used to calculate the rms charge radii of the calcium isotopes using harmonic-oscillator radial wavefunctions. The number of protons excited from $(1s_{1/2}, 0d_{3/2})$ to $(0f_{7/2}, 1p_{3/2})$ showed an odd-even effect. When these orbital occupations were used with harmonic-oscillator radial wavefunctions one obtained an increase in the rms charge radii with odd-even oscillations that were in qualitative agreement with experiment. However, in [5] when the orbital occupation numbers from these calculations were used to constrain the spherical EDF calculations, the increase in the rms charge radii was small compared to experiment.

To explore the β_2^2 contributions to the charge radii

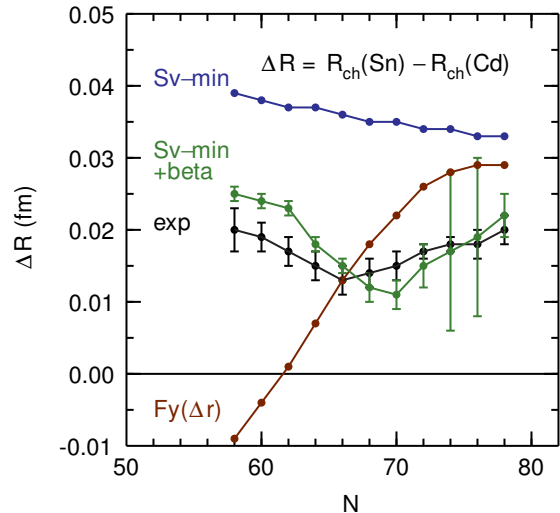


FIG. 6. Cd-Sn isotonic shifts. The experimental results from [14], and [15] are compared to the Sv-min and Fr(Δr) EDF calculations given in [14] and [15].

we will use the ZBM2-modified Hamiltonian for the $(1s_{1/2}, 0d_{3/2}, 0f_{7/2}, 1p_{3/2})$ model space as described in [46]. The corrections for the rms charge radii using the $B(E2)$ values from these calculations are shown by the blue line in panel (b) of Fig. (7). We use effective charges of $e_p = 1.22$ and $e_n = 0.78$ from [18]. There is a disagreement with the calculated and experimental $B(E2)$ for ^{46}Ca . This can be traced to the location of the $2p-2h$ proton intruder state that comes at 1.8 MeV in the calculations. Experimentally it is observed at 2.4 MeV [47]. ZBM2-modified Hamiltonian was designed for the region of ^{40}Ca . When it is used for the region of ^{48}Ca the proton shell gap is too small. This can be fixed by adding a monopole term to the Hamiltonian that moves the proton $2p-2h$ state in ^{46}Ca up to 2.4 MeV. The proton $2p-2h$ state in ^{48}Ca is suggested to be at 4.28 MeV [48] compared to the calculated excitation energy of 4.45 MeV. The results for the β_2^2 correction are shown by the green line in panel (a) of Fig. (7). EDF results for $^{49,50}\text{Ca}$ are discussed on the end of this paper.

In addition to the results for even-even nuclei obtained with $B(E\lambda, \uparrow)$, we include results for the odd-even nuclei obtained from

$$\langle i | Q \cdot Q | i \rangle = \frac{1}{(2J_i + 1)} \sum_{c \neq i} \langle i || Q || c \rangle \langle c || Q || i \rangle, \quad (6)$$

where Q is the $E2$ operator. For even-even nuclei this is $B(E2, \uparrow)$. The sum for odd-even nuclei is typically over many excited states. For example, in ^{43}Ca , there are 11 excited states below 3.5 MeV that contribute.

The odd-even effects in the orbital occupations and β_2^2 values are implicitly connected to the pairing interaction. But the specific connections between the pairing oscillations in the nuclear binding energies and the rms charge radii depends upon details of the local nuclear structure. There are many contributions to consider for rms radii: the properties of the EDF functional, orbital occupations, β_2^2 corrections, and possible pairing-type additions to the EDF. Our results suggest that the spherical EDF together with the β_2^2 corrections are the most important. But at a quantitative level of detail, all must be considered.

ISOTONIC SHIFTS FOR THE $N = 28$ ISOTONES

The results for the $N = 28$ isotones obtained with the GXPF1A Hamiltonian for $N = 28$ are shown by the green line in Fig. (8). We use effective charges of $e_p = 1.22$ and $e_n = 0.78$ from [18] and the β_2^2 model of [18] that includes the isovector term. One observes odd-even oscillations in the calculated results. The β_2^2 contribution only includes the 2_1^+ state. These are the calculations that were used to make the β_2^2 corrections for the connecting the mirror charge radii of ^{54}Ni and ^{54}Fe to the slope parameter L of neutron equation of state in [18]. As noted in [18], for ^{54}Fe there is additional $E2$ strength at 2.8 MeV in the fp calculation. This is not included because it comes from coupling of two-proton holes in ^{56}Ni to the 2^+ particle-hole excited state in ^{56}Ni at 2.7 MeV.

Charge radii calculated by the spherical EDF for $N = 28$ are linear as a function Z . Thus, to obtain the β^2 correction from experiment we can take the difference between the rms charge radius for each isotope and that obtained from a linear extrapolation between the experimental values for ^{48}Ca [11] and ^{56}Ni [13]. These results are shown by the black points in Fig. (8). More complete and improved experimental results are needed for the odd-even isotopes.

The correlation between the difference in mirror charge radii and the symmetry energy parameter L is obtained with spherical EDF [49] and CODF [50] calculations that are linear in between ^{48}Ca and ^{56}Ni . In addition, as discussed in [18], one has to add the β_2^2 corrections for ^{54}Fe as shown in Fig. (8) and for ^{54}Ni . The oscillations in the rms charge radii are treated in a different way in the Fayans-type functional by adding pairing-type functional with new global parameters [14], [15], [3]. In the Fayans method some of the correlation between the mirror charge radii and L is lost [51].

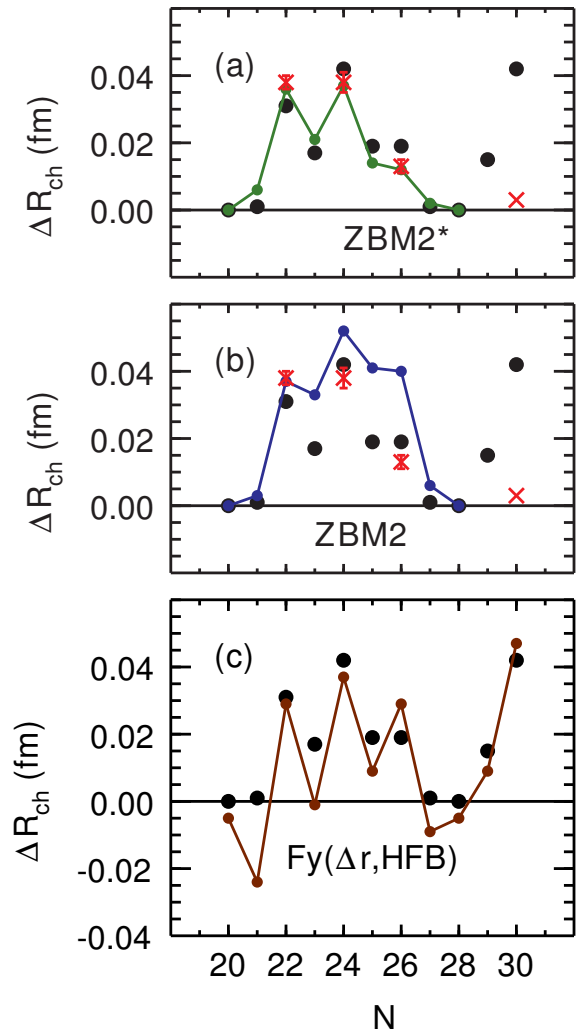


FIG. 7. ΔR_{ch} for the calcium isotopes. The black circles are the experimental results from [11] with error bars about the size of the circles. The calculations shown in panel (c) are the results from the $\text{Fy}(\Delta r, \text{HFB})$ calculations given in [44]. The lines shown in panels (a) and (b) are based on the $B(E2)$ calculations discussed in the text. The red crosses in panels (a) and (b) are based on experimental $B(E2)$ values in the text.

INCREASE IN CHARGE RADII AFTER THE MAGIC NUMBERS

Spherical EDF with β_2^2 corrections do not account for the increase in the rms charge radii just after the magic numbers shown in the bottom of Figs. (2), (3) and (7). All of these increases are associated with the sudden occupation of the orbitals with an addition node given in Table I. The experimental difference in the rms charge radii between ^{49}Ca and ^{48}Ca is given in Table II and compared with results of some calculations. The result

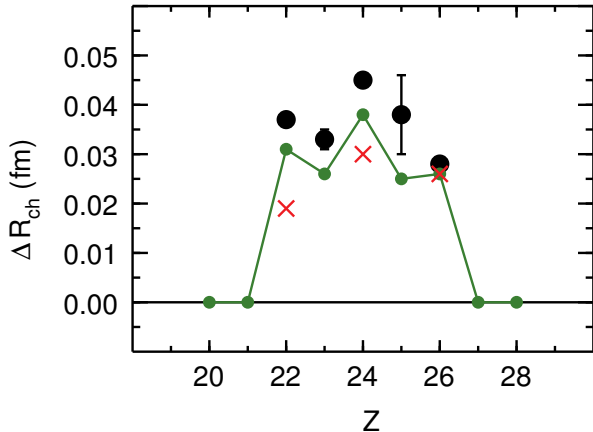


FIG. 8. ΔR_{ch} obtained from β_2^2 corrections for the isotones with $N = 28$ isotopes. The red crosses are based on experimental $B(E2, 0_1^+ \rightarrow 2_1^+)$ values. The calculations shown by the green lines are discussed in the text. The experimental data differences between the given isotope and a linear extrapolation between ^{48}Ca [11] and ^{56}Ni [13]. The data for $Z = 22, 23, 24$ and 26 are from [10] using combined analyses of the muonic-X ray and electron scattering measurements, where they are available. Otherwise only the electron scattering data is used. The charge radius for $Z = 25$ is from [9]. Charge radii for $Z = 21$ and 27 are not experimentally known yet.

for the covariant density functional (CODF) model are taken as one quarter of the increase between ^{52}Ca and ^{48}Ca shown in Fig. 24 of [2]. Nuclear matter densities for ^{40}Ca , ^{48}Ca and ^{52}Ca obtained with the $s17$ EDF parameter set are shown in Fig. (9). The interior densities show a large variation. In particular, the matter density for ^{52}Ca has a larger interior density due to the node in the radial wavefunctions. The "size" of the nucleus is determined by the interior saturation conditions imposed by the EDF functional. Perhaps the present generation of EDF functionals are not complex enough to correctly take into account these variations in the interior shape.

It is noted in [52] that the orbitals given in Table I are all associated with a sudden change in the octupole instabilities via their large $B(E3)$ values with higher orbitals that differ by $\Delta j = 3, 0g_{9/2}, 0h_{11/2}, 0i_{13/2},$ and $0j_{15/2}$, respectively (see Fig. 2 in [52]). This results in a sudden increase in the $B(E3)$ just after the magic numbers. This may contribute to the increase in the ΔR_{ch} observed in the bottom of Figs. (2) and (3). The $E3$ contribution from the $(0p_{3/2})^n$ configurations for ^{48+n}Ca would increase linearly with n . The $E3$ contribution from the $(0d_{5/2})^n$ configurations for ^{90+n}Zr would be maximized in ^{96}Zr where a peak in the $E3$ contribution to ΔR_{ch} is observed in Fig. (4). The octupole contributions to the rms radii in an EDF model that includes octupole degrees of freedom [52], [53] needs to be explored.

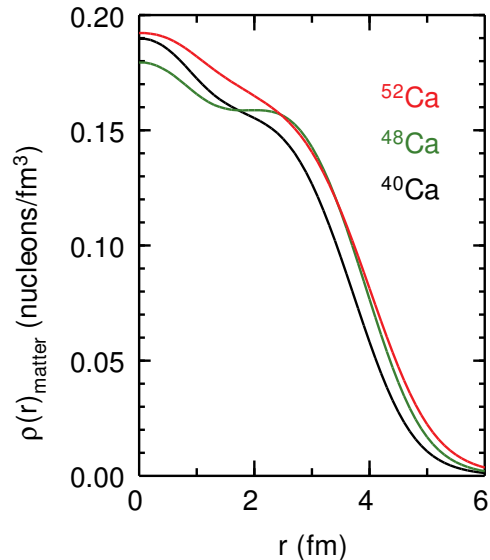


FIG. 9. Nuclear matter densities obtained with the $s17$ EDF parameters.

TABLE I. Experimental increase in the rms charge radii after the magic numbers.

N	orbital	Nuclei	ΔR_{ch} (fm)
28	$1p_{3/2}$	$^{49-48}\text{Ca}$	0.015(3)
50	$1d_{5/2}$	$^{91-90}\text{Zr}$	0.015(2)
82	$1f_{7/2}$	$^{133-132}\text{Sn}$	
132	$1g_{9/2}$	$^{209-208}\text{Pb}$	0.009(2)

CONCLUSIONS

In this paper we considered the β_λ^2 corrections to rms radii provided by the Bohr model. We showed results for $\lambda=2, 3$ and 4 . The most important β_2^2 contribution can be obtained from experimental $B(E2)$ value. When these β_2^2 corrections are added to spherical EDF calculations, the rms charge radii for even-even nuclei are in

TABLE II. Charge rms difference between ^{49}Ca and ^{48}Ca in units of (fm)

$\Delta R_{ch}(\text{exp})$	Ref.	0.015(3)
Sv-min	[44]	0.008
s8	[4]	0.009
s17	[4]	0.010
CODF	[2]	0.011
M3Y-P6a	[31]	0.011
Fy(Δr ,BCS)	[44]	0.004
Fy(Δr ,HFB)	[44]	0.014

reasonable agreement with experiment. The major deviations between theory and experiment appear just after the magic numbers. We also used the experimental $B(E2)$ to calculate the isotonic shift between the cadmium and tin isotopes, the isotopic shifts of the calcium isotopes and the isotonic shifts of the $N = 28$ isotones. The results are all in reasonable agreement with the data.

For the calcium isotopes and the $N = 28$ isotones, we used configuration-mixing calculations to obtain the $\langle Q \cdot Q \rangle$ corrections for both even-even and odd-even nuclei. The calculated $B(E2)$ for even-even nuclei are in reasonable agreement with experiment. The evaluation of $\langle Q \cdot Q \rangle$ for the odd-even nuclei leads to odd-even oscillations in the rms charge radii that are also in reasonably good agreement with the data.

For the β_2^2 correction model, the primary remaining deviation between experimental and theoretical rms charge radii is for the rapid increase just after the magic numbers. We suggest that this may come from octupole deformations and/or a limitation in the standard form of the Skyrme-type EDF functionals.

This work was supported by NSF grant PHY-2110365 and NSF PHY 2111185. We thank H. Nakada and W. Nazarewicz for discussions and suggestions.

-
- [1] M. Kortelainen, Z. Sun, G. Hagen, W. Nazarewicz, T. Papenbrock, and P.-G. Reinhard, Phys. Rev. C **105**, L021303 (2022).
- [2] U. C. Perera, A. V. Afanasjev, and P. Ring, Phys. Rev. C **104**, 064313 (2021).
- [3] P.-G. Reinhard and W. Nazarewicz, Phys. Rev. C **95**, 064328 (2017).
- [4] B. A. Brown and A. Schwenk, Phys. Rev. C **89**, 011307(R) (2014).
- [5] D. M. Rossi et al., Phys. Rev. C **92**, 014305 (2015).
- [6] A. Volya, B. A. Brown and V. Zelevinsky, Phys. Lett. B **509**, 37 (2001).
- [7] B. A. Brown, C. Bronk and P. E. Hodgson, Jour. Phys. G **10**, 1683 (1984).
- [8] J.-P. Delaroche, M. Girod, J. Libert, H. Gouffé, S. Hilaire, S. Peru, N. Pillet, and G. F. Bertsch, Phys. Rev. C **81**, 014303 (2010).
- [9] I. Angeli and K. P. Marinova, Atomic Data and Nucl. Data Tables **99**, 69 (2013).
- [10] G. Fricke and K. Heilig, Nuclear Charge Radii (Springer, Berlin Heidelberg, 2004).
- [11] R. F. Garcia Ruiz, Nature Physics **12**, 594 (2016).
- [12] K. Minamisono et al., Phys. Rev. Lett. **117**, 252501 (2016).
- [13] F. Sommer et al., to be published.
- [14] M. Hammen et al., Phys. Rev. Lett. **121**, 102501 (2018).
- [15] C. Gorges et al., Phys. Rev. Lett. **122**, 192502 (2019).
- [16] A. Bohr and B. R. Mottelson, *Nuclear Structure vol. I*, (New York: Benjamin. 1969).
- [17] H. Esbensen and G. F. Bertsch, Phys. Rev. C **28**, 355 (1983).
- [18] S. V. Pineda et al., Phys. Rev. Lett. **127**, 182503 (2021).
- [19] J. Dobaczewski, P. Vogel and A. Winter, Phys. Rev. C **29**, 1540 (1984).
- [20] S. A. Ahmad, W. Klempt, R. Neugart, E. W. Otten, P.-G. Reinhard, G. Ulm, and K. Wendt, Nucl. Phys. A **483**, 244 (1988).
- [21] G. F. Bertsch, Eur. Phys. J. A **55**, 248 (2019).
- [22] B. A. Brown, Phys. Rev. C **58**, 220 (1998).
- [23] B. A. Brown, Phys. Rev. Lett. **111**, 232502 (2013).
- [24] P. Kluepfel, P.-G. Reinhard, T. J. Buervenich, and J. A. Maruhn Phys. Rev. C **79**, 034310 (2009).
- [25] S. Fayans, S. Tolokonnikov, E. Trykov, and D. Zawischa, Nucl. Phys. A **676**, 49 (2000).
- [26] E. E. Saperstein and S. V. Tolokonnikov, Phys. At. Nucl. **74**, 1277 (2011).
- [27] B. Pritychenko, M. Birch, B. Singh, and M. Horoi, Atomic Data and Nucl. Data Sheets **107**, 1 (2016).
- [28] J. W. Lightbody, S. Penner, and S. P. Fivozinsky, P. L. Hallowell and H. Cranne, Phys. Rev. C **14**, 952 (1976).
- [29] R. H. Spear and W. N. Catford, Phys. Rev. C **41**, R1351 (1990).
- [30] S. Goriely, N. Chamel and J. M. Pearson, Phys. Rev. C **88**, 061302(R) (2013).
- [31] H. Nakada, Phys. Rev. C **92**, 044307 (2015), and private communication.
- [32] B. Pritychenko, M. Birch, and B. Singh, Nucl. Phys. A **962**, 73 (2017)
- [33] I. Talmi, Nucl. Phys. A **423**, 189 (1984).
- [34] L. Zamick, Phys. Rev. C **82**, 057304 (2010).
- [35] M. Horoi, Phys. Rev. C **50**, 2384 (1994).
- [36] L. Zamick, Zeit. fur Phys. A **327**, 409 (1987).
- [37] E. Caurier, K. Langanke, G. Martinez-Pinedo, F. Nowacki and P. Vogel, Phys. Lett. B **522**, 240 (2001).
- [38] D. Zawischa, Phys. Lett. B **155**, 309 (1985).
- [39] F. Barranco and R. A. Broglia, Phys. Lett. B **15**, 1, 90 (1985).
- [40] W. R. Gibbs and J. P. Dedonder, Phys. Rev. C **46**, 1825 (1992). pion scattering and matter radii for Ca
- [41] K. Hadynska-Klek, Phys. Rev. C **97**, 024326 (2018).
- [42] C. E. Towsley, D. Cline and R. N. Horoshko, Nucl. Phys. A **204**, 574 (1973).
- [43] J. J. Valiente-Dobon et al., Phys. Rev. Lett. **102**, 242502 (2009).
- [44] A. J. Miller et al., Nat. Phys. **15**, 432 (2019).
- [45] B. Longfellow, D. Weisshaar, A. Gade, B. A. Brown, D. Bazin, K. W. Brown, B. Elman, J. Pereira, D. Rhodes, and M. Spieker, Phys. Rev. C **103**, 054309 (2021).
- [46] M. L. Bissell et al., Phys. Rev. Lett. **113**, 052502 (2014).
- [47] W. Kutschera, B. A. Brown, H. Ikezoe, G. D. Sprouse, Y. Yamazaki, Y. Yoshida, T. Nomura and H. Ohnuma, Phys. Rev. C **12**, 813 (1975).
- [48] B. A. Brown and W. A. Richter, Phys. Rev. C **58**, 2099 (1998).
- [49] B. A. Brown, Phys. Rev. Lett. **119**, 122502 (2017).
- [50] J. Yang and J. Piekarewicz, Phys. Rev. C **97**, 014314 (2018).
- [51] P.-G. Reinhard and W. Nazarewicz, Phys. Rev. C **105**, L021301 (2022).
- [52] W. Nazarewicz, P. Oleadners, I. Ragnarsson, J. Dudek, G. A. Leander, P. Moeller, R. Ruchowka, Nucl. Phys. A **429**, 269 (1984).
- [53] Y. Cao, S. E. Agbemava, A. V. Afanasjev, W. Nazarewicz, and E. Olsen, Phys. Rev. C **102**, 024311 (2020).